Pressure-dependent transition in protein dynamics at about 4 kbar revealed by molecular dynamics simulation

Lars Meinhold and Jeremy C. Smith
Computational Molecular Biophysics, Interdisciplinary Center for Scientific Computing (IWR), University of Heidelberg, Im Neuenheimer Feld 368, D-69120 Heidelberg, Germany
(Received 29 July 2005; published 13 December 2005)

Molecular dynamics simulations of a crystalline protein, *Staphylococcal* nuclease, over the pressure range 1 bar to 15 kbar reveal a qualitative change in the internal protein motions at ≈4 kbar. This change involves the existence of two linear regimes in the mean-square displacement for internal protein motion, $\langle u^2 \rangle(P)$ with a twofold decrease in the slope for $P>4$ kbar. The major effect of pressure on the dynamics is a loss, with increasing pressure of large amplitude, collective protein modes below 2 THz effective frequency, accompanied by restriction of large-scale solvent translational motion.

DOI: 10.1103/PhysRevE.72.061908 PACS number(s): 87.14.Ee, 62.50.+p, 87.15.He, 87.64.Bx

I. INTRODUCTION

The temperature dependence of internal protein dynamics has been much studied and has yielded valuable information on the energy landscape underlying protein function [1–3]. In comparison, relatively few studies have been performed investigating the dependence of protein dynamics on pressure [4–6]. Pressure-induced structural changes have been reported for deoxymyoglobin [7], lysozyme [8–10], BPTI [11], myoglobin [12], and ubiquitin [13], and pressure-induced unfolding in solution has been reported for *Staphylococcal* nuclease (SNase) [14–17], myoglobin [18], α-lactalbumin [19], and various other proteins [20]. Hydration water has been suggested to play a key role in high-pressure protein unfolding, as indicated by structural and dynamical changes in the protein:water interface and the penetration of water molecules into the hydrophobic core [11,17,18,21,22]. Pressure-induced dynamical changes have hitherto been relatively neglected, although in early molecular dynamics (MD) simulations of small proteins a reduction of positional fluctuations of protein atoms was found upon the application of pressure [11,21,23].

Here, results from MD simulations of crystalline SNase in the pressure range 1 bar to 15 kbar are presented. The advantage of the crystalline state over solution is that steric constraints imposed by the crystalline environment hinder denaturation, as has been demonstrated for orthorhombic crystals of lysozyme, which remain stable up to 10 kbar [24]. SNase was chosen here as it is experimentally well characterised and because crystals of the protein also remain structurally stable at pressures at which SNase in solution is partly unfolded [25].

II. MODEL DESCRIPTION AND VALIDATION

The present MD simulations were performed using the CHARMM program (version 28b1, parameter set 22) [26,27]. Details of the simulation setup have been reported previously [28]. The primary simulation cell is composed of one tetragonal crystal unit cell with initial dimensions $48.5\times48.5\times63.4$ Å^3 containing four protein molecules arranged in the space-group symmetry $P4_1$, 2115 TIP3P [29] water molecules, and 48 chloride counter ions. Periodic boundary conditions were applied in the simulation so as to generate the correct infinite crystal environment. Constant-pressure constant-temperature simulations were performed using the Nosé-Hoover algorithm [30–32]. This algorithm does not produce the exact isothermal-isobaric (*NPT*) ensemble [32–34] for which the the average internal pressure equals the externally applied pressure $\langle P_{\mathrm{int}} \rangle = P_{\mathrm{ext}}$ but rather yields $\langle P_{\mathrm{int}} \rangle_{\mathrm{NH}} = P_{\mathrm{ext}} + k_B T \langle V^{-1} \rangle$ [34]. Therefore, for a large system, as is simulated here, the Nosé-Hoover algorithm provides a good approximation of the *NPT* ensemble. The system was equilibrated for 10.2 ns at 300 K and 1 bar, then pressurised at a rate of 1 kbar ns^{-1} and subsequently equilibrated for 200 ps. The production phase of each simulation was 1 ns long.

The unit-cell volume decreased nonlinearly with increasing P, the reduction from 1 bar to 15 kbar being 15%. The compressibility, $\beta = \partial(\ln V)/\partial P$ reduced from 28 ± 11 Mbar^{-1} at 1 bar to 6.6 ± 2.8 Mbar^{-1} at 15 kbar with a mechanical nonlinearity index $\mu = \partial\beta^{-1}/\partial P = 9.1\pm0.4$. These values are within the experimental ranges of estimates for β (10–20 Mbar^{-1}) and μ (0–10) reported for the P dependence of the unit-cell volume in lysozyme crystals [24,35,36].

The protein radius of gyration decreased by 3.5 ± 0.5% from 1 bar to 15 kbar, leading to an estimated reduction of the protein volume of 10%. Therefore, the protein compressibility is significantly smaller than that of the unit cell, and thus also the water compressibility, which is again consistent with previous findings [4]. The decrease of solvent volume is manifested by a shift to shorter distances of the nearest-neigbor peak in the solvent radial distribution function, corresponding to a decrease in the average nearest-neighbor distance of 0.7% from 1 bar to 15 kbar (results not shown).

The root mean-square deviation of the average simulation structure from the experimental (300 K, 1 bar) crystal structure [37] showed little variation with increasing P, the average over all four proteins in the unit cell being 2.2 ± 0.3 and 2.3 ± 0.3 Å at 1 bar and 15 kbar, respectively. Also, the secondary structural elements were conserved throughout the

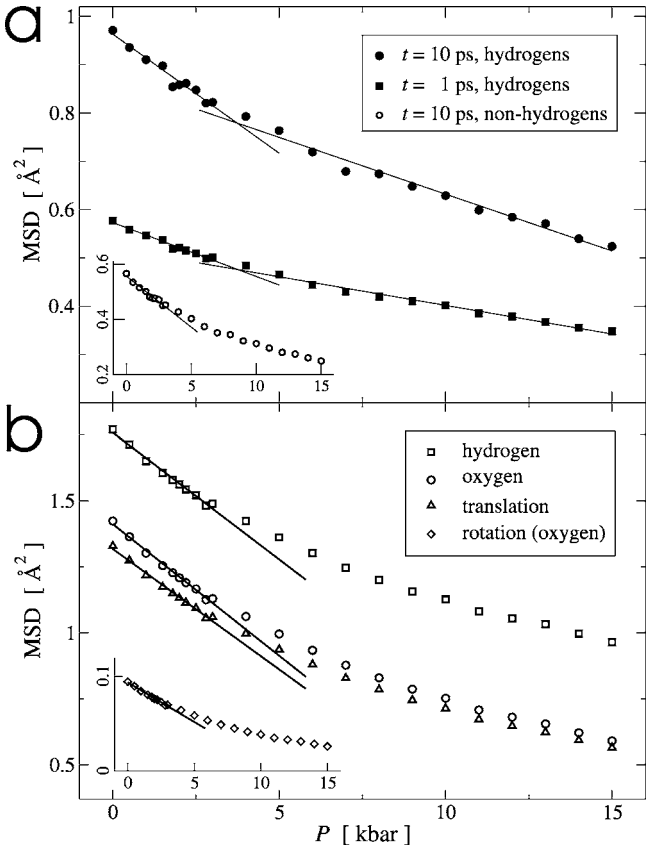

FIG. 1. (a) Mean-square displacement $\langle u^2 \rangle$ averaged over all protein hydrogen atoms on two time scales t. The lines show linear fits performed over the ranges $P \leqslant 3$ kbar and $P \geqslant 4$ kbar. The shape of $\langle u^2 \rangle(P)$ is similar for $t=100$ ps (data not shown) and for nonhydrogen protein atoms (shown in the inset). (b) $\langle u^2 \rangle(P)$ for $t=1$ ps averaged over all solvent hydrogens and oxygens, respectively. For the oxygens, the decomposition into translation and rotation $\langle u^2 \rangle = \langle u^2 \rangle_T + \langle u^2 \rangle_R$ is also shown. The lines represent linear fits performed in the low-P regime.

simulations. The ensemble of the above findings indicate that the protein and simulation system were stable at all pressures and that pressure-related structural features agree within error with experiment.

III. RESULTS AND DISCUSSION

A convenient measure for the overall motion present in a protein molecule is provided by the time-dependent mean-square displacement

$$\langle u^2 \rangle(t) = \overline{\langle [\mathbf{r}_k(\tau) - \mathbf{r}_k(\tau + t)]^2 \rangle}, \tag{1}$$

where $\mathbf{r}_k(\tau)$ is the coordinate vector of atom k at time τ, $\langle \cdots \rangle$ is the time average and the overbar the average over the protein atoms. In Fig. 1(a), $\langle u^2 \rangle(t)$ for the internal motion is plotted against P for two values of t: 1 and 10 ps. On both time scales $\langle u^2 \rangle$ significantly decreases with increasing pressure, with the reduction between 1 bar and 15 kbar for hydrogens being 46 and 40% for $t=1$ and 10 ps, respectively.

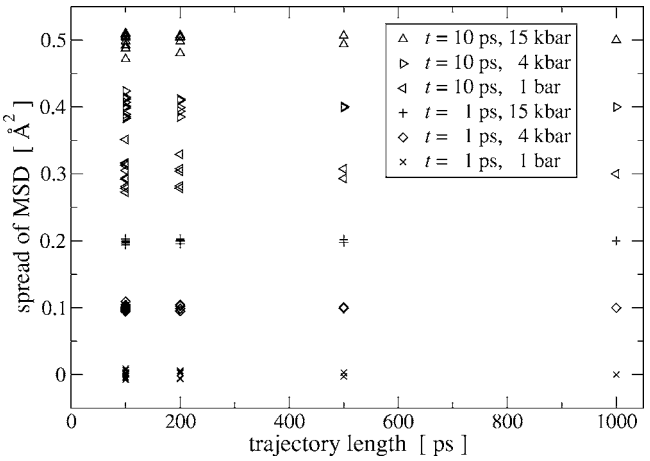

FIG. 2. Spread of the mean-square displacements dependent on the trajectory length for two time scales t and three pressure values P. The calculation included all protein hydrogen atoms. For clarity, for each set of t and P the results were shifted along the y axis by an arbitrary constant.

For nonhydrogen atoms, shown in the inset to Fig. 1(a), the reduction is larger, being 56% for $t=10$ ps. The slope of $\langle u^2 \rangle(P)$ is linear in two distinct ranges of P, with a broad transition around $P^* \approx 4$ kbar. In the regimes below and above P^*, referred to in the following as "low-P" and "high-P," respectively, linear regressions were performed and are also shown in Fig. 1(a). For both values of t, in the low-P regime the slope is higher by a factor of ≈ 2 than in the high-P regime. This nonlinearity in $\langle u^2 \rangle(P)$ indicates a qualitative change in protein dynamics upon pressurization. This nonlinearity is reminiscent of the much-studied transition in $\langle u^2 \rangle(T)$, which involves a solvent-driven activation of anharmonic protein dynamics with increasing T at ≈ 200 K, leading to a nonlinear increase in the average atomic mean-square displacement $\langle u^2 \rangle(T)$ [38–40].

The solvent $\langle u^2 \rangle(P)$ [Fig. 1(b)] is dominated by translational diffusion. Both the translational and rotational $\langle u^2 \rangle$ decrease linearly with P below P^* and nonlinearly, at a lower rate, above P^*. At all pressures, $\langle u^2 \rangle(t) \propto t^\alpha$ with $\alpha < 1$, indicating subdiffusion [41]. α exhibits no significant P-dependence, the average calculated over all simulations being 0.86 ± 0.01, a value intermediate between that of protein hydrational water, for which $\alpha \approx 0.6$ [42], and bulk water ($\alpha = 1$).

To estimate the statistical errors associated with the values of $\langle u^2 \rangle$ given in Fig. 1, at selected values of P (1 bar, 4 kbar, and 15 kbar) each trajectory was divided into nonoverlapping subtrajectories, for each of which $\langle u^2 \rangle$ was recalculated using Eq. (1). The results of this analysis using $t=1$ ps and 10 ps and several lengths of the subtrajectories are shown for the protein hydrogen atoms in Fig. 2. For all values of P, the spread in $\langle u^2 \rangle$ is very small for $t=1$ ps, the relative standard deviation being smaller than 1% for the subtrajectory length 100 ps. For $t=10$ ps, the relative standard deviation is below 2.5% for the subtrajectory length 100 ps but is seen to significantly reduce for longer time scales. The statistical errors associated with the results presented in Fig. 1 can, therefore,

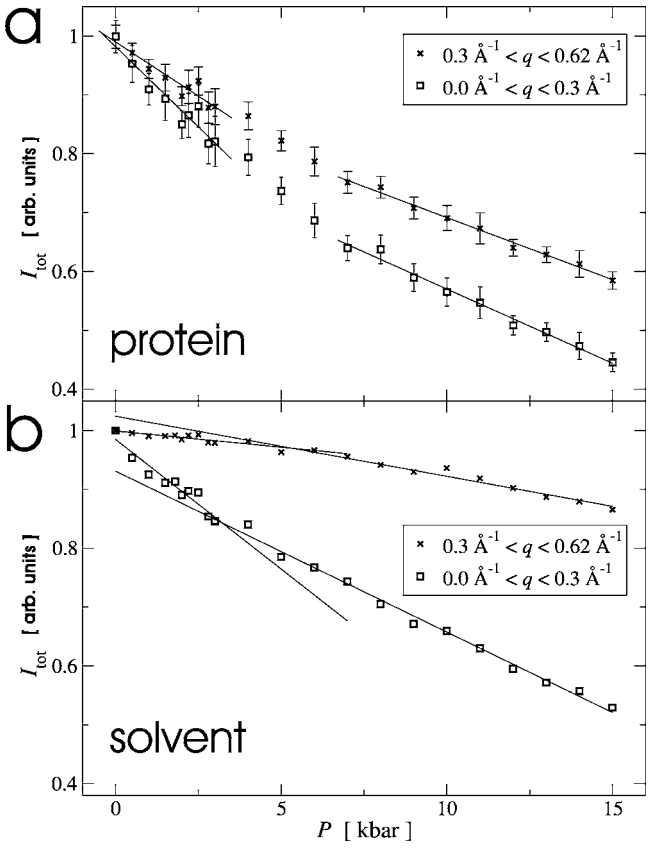

FIG. 3. Protein (a) and solvent (b) x-ray diffuse scattering intensities I_{tot} integrated over two ranges of the magnitude q of the scattering vector. I_{tot} is normalized such that $I_{\mathrm{tot}}(1\ \mathrm{bar})=1$. The solvent I_{tot} was calculated from the full trajectory (1 ns). Since protein x-ray diffuse scattering does not converge on the ns time scale [28], for each P the protein I_{tot} was estimated from ten non-overlapping 100 ps subtrajectories and the error bars denote the standard deviation. The lines show linear fits in the low- and high-P (for the protein: $P \geqslant 7$ kbar) regimes, respectively.

be estimated to be approximately 0.3 and 0.8% for $t=1$ and 10 ps, respectively. Thus, the finding of the nonlinear change in $\langle u^2\rangle(P)$ is statistically significant.

To examine which protein and solvent motions are affected by the pressure increase the P dependence of the x-ray diffuse scattering intensity, $I(\mathbf{q})$ was calculated as [43]

$$I(\mathbf{q}) = I_{\mathrm{tot}}(\mathbf{q}) - I_{\mathrm{Bragg}}(\mathbf{q}) \propto \langle |F|^2 \rangle - |\langle F \rangle|^2, \qquad (2)$$

where F is the instantaneous structure factor, $F = \Sigma_k f_k e^{i\mathbf{q}\cdot(\mathbf{r}_k+\mathbf{u}_k)}$, f_k and $\mathbf{r}_k$ are the form factor and the mean position vector of the kth atom, respectively, $\mathbf{u}_k$ is the displacement vector of atom k from $\mathbf{r}_k$, and k runs over all protein or solvent atoms in the unit cell. $I(\mathbf{q})$ indicates the amplitude of collective motion present on the length scale q^{-1}. Here, $I(\mathbf{q})$ was calculated for 55 691 values of $\mathbf{q}$ in the range $\|\mathbf{q}\| < 0.62$ Å^{-1}. This range was divided into a low-q range $q < 0.3$ Å^{-1}, probing large-scale collective motions, and a high-q range $q > 0.3$ Å^{-1}, probing more local dynamics. $I(\mathbf{q})$ was integrated over each range to yield the total intensity I_{tot} which is plotted against P in Fig. 3.

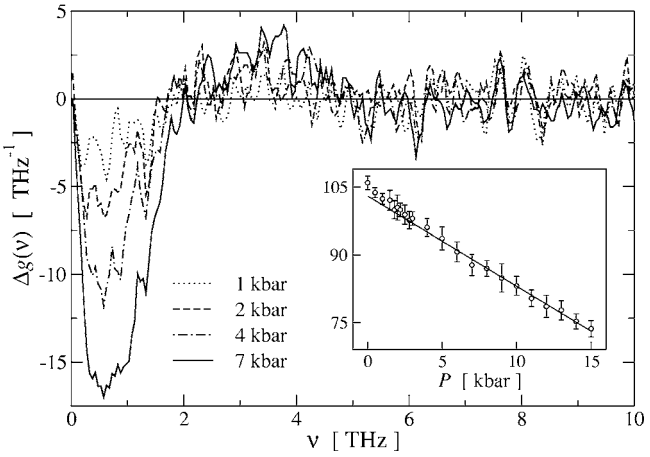

FIG. 4. Change in the vibrational density of states, $\Delta g(\nu)$ for selected pressure values. $\Delta g(\nu)$ was calculated as the difference $g_P(\nu) - g_{P_0}(\nu)$, with the reference pressure $P_0=1$ bar. The inset shows the number of modes with $\nu \leqslant 2$ THz with a linear fit to the high-P regime. The gradient in the low- and high-P regime is -2.6 ± 0.2 and -1.99 ± 0.06 kbar^{-1}, respectively. Results shown are averaged over all four proteins in each simulation.

In both q ranges, the protein and solvent $I_{\mathrm{tot}}(P)$ vary approximately linearly with P below and above P^* and thus support the above finding of a pressure induced dynamical transition. $I_{\mathrm{tot}}(P)$ for the protein [Fig. 3(a)] decreases faster in the low-q range [with gradients of -0.055 ± 0.007 kbar^{-1} (low-P) and -0.025 ± 0.001 kbar^{-1} (high-P)] than in the high-q range [with gradients of -0.037 ± 0.005 kbar^{-1} (low-P) and -0.021 ± 0.001 kbar^{-1} (high-P)], indicating that, upon the application of pressure, large-scale collective displacements are more strongly suppressed than the local dynamics. $I_{\mathrm{tot}}(P)$ calculated for the crystal solvent is shown in Fig. 3(b). In the low-q range the solvent $I_{\mathrm{tot}}(P)$ strongly decreases with increasing P, the rate of decrease being larger in the low-P regime. At low q, the large-scale collective displacements, $I_{\mathrm{tot}}(P)$ of the protein and the solvent reduce approximately equally, reaching 0.45 ± 0.02 and 0.53, respectively at $P=15$ kbar. This indicates that large-scale collective motions of the protein and collective translational solvent dynamics are similarly affected by high pressure, consistent with previous work suggesting strong coupling between solvent dynamics and large-scale protein motion [44–47]. In contrast, the P dependence of the high-q, short length-scale motion differs significantly between the protein and the solvent: whereas the protein I_{tot} reaches 0.59 ± 0.01 at $P=15$ kbar that of the solvent reduces to only 0.86. Furthermore, the change in the solvent I_{tot} is negligible up to ≈ 4 kbar, indicating that the local dynamics of water remains roughly unchanged in the low-P regime. This is consistent with previous work indicating that, at ambient temperature and low P, water mobility is controlled by the tetrahedral ordering due to hydrogen bonds whereas, at higher P, the tetrahedral ordering breaks down and the dynamics is controlled by the van der Waals repulsion of neighboring molecules [48–50].

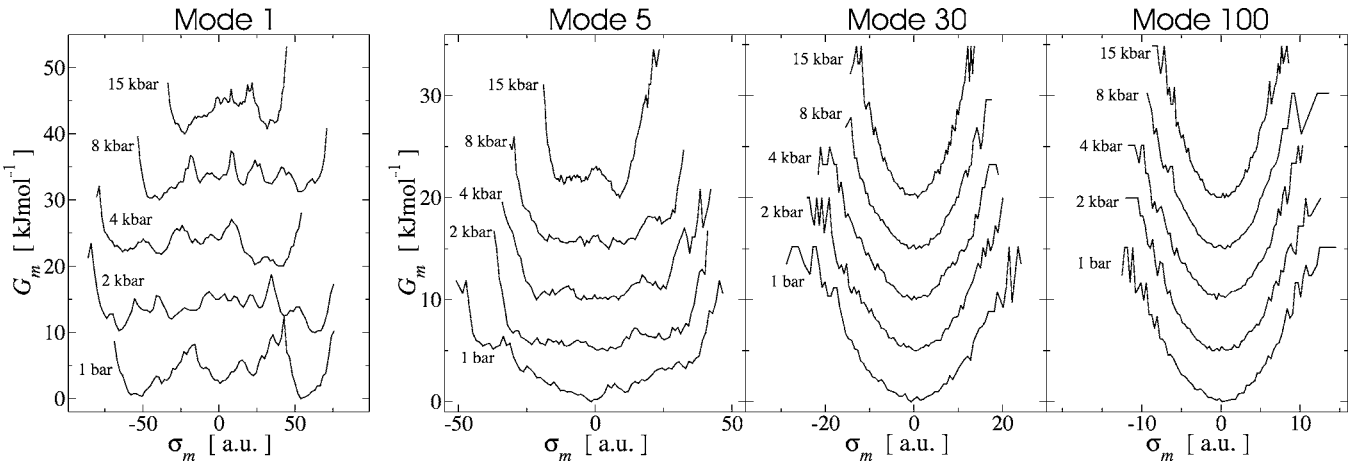

FIG. 5. Pressure dependence of the effective free energy profiles G_m of selected PCA modes at various values of P. For clarity, in each graph the profiles are separated along the y axis by a constant (10 kJ mol^{-1} for mode 1 and 5 kJ mol^{-1} for the other modes).

The protein collective motions were further dissected using principal component analysis (PCA). In PCA the mass-weighted variance-covarience matrix is diagonalized, yielding the eigenvectors $\mathbf{v}_m$, which determine the direction of a collective mode, and their associated eigenvalues, which are related to the associated eigenfrequency ν_m. From ν_m the vibrational density of states, $g(\nu)$ was calculated for each simulation. The change in $g(\nu)$ upon application of pressure is illustrated in Fig. 4. With increasing P the number of modes with frequencies $\nu \lesssim 2$ THz strongly decreases, the rate of decrease exhibiting a small nonlinearity at P^* (inset to Fig. 4). Low-frequency modes are thus shifted into the higher-frequency range. These low-frequency modes have been shown to be mostly collective, anharmonic and distributed over the whole protein [40,51].

It is of interest to investigate the form of the effective free energy profiles, G_m associated with the PCA modes and, in particular, whether the P-dependent dynamical transition found above is accompanied by a loss of anharmonic motion similar to that seen in the T-dependent dynamical transition [40]. The effective free energy along mode m is given by

$$G_m(\sigma) = -k_B T \ln p_{\sigma_m}, \tag{3}$$

where the projection, $\sigma_m(t)$ of the trajectory onto the mode is defined as

$$\sigma_m(t) = [M^{1/2}\mathbf{u}^T(t)] \cdot \mathbf{v}_m \tag{4}$$

and depends on the instantaneous displacement vector $\mathbf{u}(t)$ of all atoms. $p_{\sigma_m} d\sigma$ is the probability that $\sigma_m(t)$ adopts a value in the interval $[\sigma, \sigma + d\sigma)$. If the motion is harmonic, then $G_m(\sigma)$ is also harmonic and the probability density, p_{σ_m} is Gaussian. In Fig. 5 the effective free energy profiles G_m for selected PCA modes (mode numbers $m = 1$, 5, 30 and 100) at various pressure values ($P = 1$ bar and 2, 4, 8 and 15 kbar) are shown. At all values of P the lowest-frequency, largest-amplitude principal component mode is anharmonic and possesses multiple substates separated by barriers with heights up to approximately 10 kJ mol^{-1}. The P-dependent dynamical transition found above is, therefore, not accompanied by a complete loss of anharmonic motions in the pressure range up to 15 kbar. With increasing mode number m, for all values of P the modes initially remain anharmonic but with the number of substates reducing until G_m becomes quasiharmonic or harmonic at $m \approx 10$ or $m \approx 30$, respectively. The effect of elevated pressure is similar for all modes: upon the application of pressure the width of G_m reduces, corresponding to an increase of the effective force constant associated with each mode.

IV. CONCLUSIONS

The present MD simulations of a crystalline protein in the pressure range 1 bar to 15 kbar have revealed the existence of a pressure-dependent transition in internal protein dynamics at ≈ 4 kbar. The transition is manifested by the existence of two linear regimes in $\langle u^2 \rangle(P)$. The major effect of pressure is a loss, with increasing pressure of large-amplitude, collective modes below 2 THz effective frequency.

The crystalline environment used here may strongly influence the protein dynamics and, in particular, prevents pressure-induced unfolding at medium pressure values. Therefore, further investigations are required to elucidate whether the pressure-induced changes in the protein dynamics found here are also present in aqueous solution. Also, as an increasing number of high-pressure non-native protein structures becomes available [7–13] it will be of interest to perform simulations to investigate whether the pressure-induced changes in protein dynamics revealed here are limited to the close-to-native region of the energy landscape. Further characterization of the dynamics below and above the pressure dynamical transition using a variety of experimental scattering and spectroscopic techniques promises to shed further light on the physics of protein energy landscapes.

[1] H. Frauenfelder, S. G. Sligar, and P. G. Wolynes, Science **254**, 1598 (1991).
[2] F. G. Parak and G. U. Nienhaus, ChemPhysChem **3**, 249 (2002).
[3] F. G. Parak, Rep. Prog. Phys. **66**, 103 (2003).
[4] K. Heremans and L. Smeller, Biochim. Biophys. Acta **1386**, 353 (1998).
[5] E. Paci, Biochim. Biophys. Acta **1595**, 185 (2002).
[6] S. M. Gruner, in *High-Pressure Crystallography*, edited by A. Katrusiak and P. McMillan (Kluwer Academic Publisher, Netherlands, 2004).
[7] T. Yamato, J. Higo, Y. Seno, and N. Gō, Proteins **16**, 327 (1993).
[8] E. Paci and M. Marchi, Proc. Natl. Acad. Sci. U.S.A. **93**, 11 609 (1996).
[9] K. Akasaka, T. Tezuka, and H. Yamada, J. Mol. Biol. **271**, 671 (1997).
[10] M. Refaee, T. Tezuka, K. Akasaka, and M. P. Williamson, J. Mol. Biol. **327**, 857 (2003).
[11] B. Wroblowski, J. F. Diaz, K. Heremans, and Y. Engelborghs, Proteins **25**, 446 (1996).
[12] P. Urayama, G. N. Phillips, Jr., and S. M. Gruner, Structure (London) **10**, 51 (2002).
[13] R. Kitahara, S. Yokoyama, and K. Akasaka, J. Mol. Biol. **347**, 277 (2005).
[14] M. W. Lassalle, H. Yamada, and K. Akasaka, J. Mol. Biol. **298**, 293 (2000).
[15] J. Woenckhaus, R. Kohling, P. Thiyagarajan, K. C. Littrell, S. Seifert, C. A. Royer, and R. Winter, Biophys. J. **80**, 1518 (2001).
[16] H. Seemann, R. Winter, and C. A. Royer, J. Mol. Biol. **307**, 1091 (2001).
[17] A. Paliwal, D. Asthagiri, D. P. Bossev, and M. E. Paulaitis, Biophys. J. **87**, 3479 (2004).
[18] W. Doster and R. Gebhardt, Chem. Phys. **292**, 383 (2003).
[19] M. W. Lassalle, H. Li, H. Yamada, K. Akasaka, and C. Redfield, Protein Sci. **12**, 66 (2003).
[20] Y. O. Kamatari, R. Kitahara, H. Yamada, S. Yokoyama, and K. Akasaka, Methods **34**, 133 (2004).
[21] D. B. Kitchen, L. H. Reed, and R. M. Levy, Biochemistry **31**, 10083 (1992).
[22] G. Hummer, S. Garde, A. E. García, M. E. Paulaitis, and L. R. Pratt, Proc. Natl. Acad. Sci. U.S.A. **95**, 1552 (1998).
[23] R. M. Brunne and W. F. van Gunsteren, FEBS Lett. **323**, 215 (1993).
[24] A. Katrusiak and Z. Dauter, Acta Crystallogr., Sect. D: Biol. Crystallogr. **52**, 607 (1996).
[25] F. H. O. Osterberg, Ph.D. thesis, Princeton University, Princeton, 1996.
[26] B. R. Brooks, R. E. Bruccoleri, B. D. Olafson, D. J. States, S. Swaminathan, and M. Karplus, J. Cryst. Growth **4**, 187 (1983).
[27] A. D. MacKerell *et al.*, J. Phys. Chem. B **102**, 3586 (1998).
[28] L. Meinhold and J. C. Smith, Biophys. J. **88**, 2554 (2005).
[29] W. L. Jorgensen, J. Chandrasekhar, J. D. Madura, R. W. Impey, and M. L. Klein, J. Chem. Phys. **79**, 926 (1983).
[30] H. C. Andersen, J. Chem. Phys. **72**, 2384 (1980).
[31] S. Nosé and M. L. Klein, Mol. Phys. **50**, 1055 (1983).
[32] W. G. Hoover, Phys. Rev. A **31**, 1695 (1985).
[33] W. G. Hoover, Phys. Rev. A **34**, 2499 (1986).
[34] G. J. Martyna, D. J. Tobias, and M. L. Klein, J. Chem. Phys. **101**, 4177 (1994).
[35] C. E. Kundrot and F. M. Richards, J. Mol. Biol. **193**, 157 (1987).
[36] D. P. Kharakoz, Biophys. J. **79**, 511 (2000).
[37] M. J. Legg, Ph.D. thesis, Texas Agricultural and Mechanical University, College Station, 1977.
[38] W. Doster, S. Cusack, and W. Petry, Nature (London) **337**, 754 (1989).
[39] A. L. Tournier, J. Xu, and J. C. Smith, Biophys. J. **85**, 1871 (2003).
[40] A. L. Tournier and J. C. Smith, Phys. Rev. Lett. **91**, 208106 (2003).
[41] L. C. Malacarne, R. S. Mendes, I. T. Pedron, and E. K. Lenzi, Phys. Rev. E **63**, 030101(R) (2001).
[42] M. Marchi, F. Sterpone, and M. Ceccarelli, J. Am. Ceram. Soc. **124**, 6787 (2002).
[43] L. Meinhold and J. C. Smith, Phys. Rev. Lett. **95**, 218103 (2005).
[44] R. Abseher, H. Schreiber, and O. Steinhauser, Proteins **25**, 366 (1996).
[45] F. Merzel and J. C. Smith, Proc. Natl. Acad. Sci. U.S.A. **99**, 5378 (2002).
[46] P. W. Fenimore, H. Frauenfelder, B. H. McMahon, and F. G. Parak, Proc. Natl. Acad. Sci. U.S.A. **99**, 16047 (2002).
[47] G. Caliskan, D. Mechtani, J. H. Roh, A. Kisliuk, A. P. Sokolov, S. Azzam, M. T. Cicerone, S. Lin-Gibson, and I. Peral, J. Chem. Phys. **121**, 1978 (2004).
[48] M. R. Reddy and M. Berkowitz, J. Chem. Phys. **87**, 6682 (1987).
[49] J. Brodholt and B. Wood, J. Geophys. Res. **98**, 519 (1993).
[50] F. W. Starr, F. Sciortino, and H. E. Stanley, Phys. Rev. E **60**, 6757 (1999).
[51] A. Kitao, S. Hayward, and N. Gō, Proteins **33**, 496 (1998).